Contact to single atoms and molecules with the tip of a scanning tunnelling microscope



2008 J. Phys.: Condens. Matter 20 223001

(http://iopscience.iop.org/0953-8984/20/22/223001)

IOP Publishing Journal of Physics: Condensed Matter

J. Phys.: Condens. Matter **20** (2008) 223001 (16pp) doi:10.1088/0953-8984/20/22/223001

TOPICAL REVIEW

# Contact to single atoms and molecules with the tip of a scanning tunnelling microscope

**J Kröger, N Néel and L Limot**[1]

Institut für Experimentelle und Angewandte Physik, Christian-Albrechts-Universität zu Kiel, D-24098 Kiel, Germany

E-mail: kroeger@physik.uni-kiel.de

Received 7 January 2008, in final form 22 February 2008
Published 16 April 2008
Online at stacks.iop.org/JPhysCM/20/223001

**Abstract**

Experiments using the tip of a scanning tunnelling microscope to contact atoms and molecules adsorbed on surfaces are reviewed. Conductance quantization upon forming or breaking a contact between the tip and surfaces as well as between the tip and specifically chosen atoms and molecular orbitals is addressed. Imaging the contact area prior to and after contact measurements allows one to monitor the status of the contacted object as well as that of the contacting electrodes. Spectroscopy with the tip in contact with individual atoms or molecules reveals the reproducibility of and control over such experiments today.

(Some figures in this article are in colour only in the electronic version)

## Contents



[1] Present address: Institut de Physique et Chimie des Matériaux de Strasbourg, UMR 7504, Université Louis Pasteur, F-67034 Strasbourg, France.

## 1. Introduction

### *1.1. Motivation*

From quantum mechanics we know that properties of materials at the atomic scale differ from those of their macroscopic counterparts. In this article we focus on the electrical conductance. Currently, many experimental and theoretical investigations are devoted to achieving an understanding of how electrons are transported through atoms, atomic wires, and molecules. The reasons for this increased interest may be found in the ongoing miniaturization in the microelectronic industry. Although we are far from replacing silicon technology by so-called molecular electronics, it is important to unravel the quantum properties of conductors with nanometre dimensions and to discover new challenges which must be faced upon reducing the size.

Closely related to electron transport is the charge transfer and concomitant energy dissipation in atomic-sized contacts. These microscopic processes are considered to be at the origin of friction, adhesion, and wear at the macroscopic scale.

These two examples which undoubtedly have an impact on our everyday life may serve as a motivation for the experimental and theoretical investigations of electrical conductors with atomic dimensions.

 

### *1.2. Historical development*

This review article will mainly address ballistic electron transport through constrictions with atomic dimensions. Therefore, we find that it is useful to characterize this conductance regime. While for macroscopic systems Ohm's law is applicable, for atomic-sized conductors such simple approaches are no longer valid. Atomic-sized conductors are a limiting case of mesoscopic systems whose transport properties are influenced by quantum coherence. A measure of the preservation of quantum coherence is the phase coherence length, $L_\Phi$, which for a mesoscopic conductor is larger than its length $L$. We can further compare the length of the conductor and the elastic mean free path ($\ell$) of the electrons. If $\ell \ll L$ then the conductance is referred to as diffusive: starting from one electrode the momentum of the electrons changes a lot of times along its trajectory to the other electrode. For $\ell > L$ the electron momentum is constant and the electron motion is limited only by scattering at the boundary of the conductor. This conductance regime is referred to as ballistic.

Conductance of a point contact in the diffusive regime was studied theoretically as early as 1873 by Maxwell [1]. By solving Laplace's equation for an orifice with radius $R$ and resistivity $\varrho$ Maxwell found a conductance of $G = 2R/\varrho$. This is a classical result reflecting Ohm's law. The situation changes when the ballistic regime of transport is considered. A large potential gradient near the contact causes the electrons to accelerate within short distances. In a semiclassical approach the conductance was given by Sharvin in 1965 according to $G = e^2 k_F^2 R^2/(2h)$ with $k_F$ the Fermi wavevector, $-e$ the electron charge, and $h$ Planck's constant [2]. The conductance of a so-called quantum point contact, i.e., a contact whose width is comparable to the Fermi wavelength $\lambda_F$, was calculated by Landauer in 1957 [3]:

$$G = \mathrm{G}_0 \sum_{i,j=1}^{n} |\tau_{ij}|^2, \tag{1}$$

where $\mathrm{G}_0 = 2e^2/h$ is the quantum of conductance and the $|\tau_{ij}|^2$ specify the transmission probability of an electron incident on the contact mode $i$ and transmitted into mode $j$. Büttiker [4] has pointed out that it is possible to define another set of modes which are referred to as eigenchannels and which do not mix in the scattering region of the quantum point contact. As a consequence, in equation (1) we set $|\tau_{ij}|^2 = T_i \delta_{ij}$ with $T_i$ the transmission probability of the $i$th eigenchannel. A recipe for the transformation of an arbitrary set of channels to eigenchannels has been given by Brandbyge and Jacobsen [5]. If the cross-section of the quantum point contact varies slowly along the constriction the transmission probability $T_i$ will be either 1 or 0 [6–9]. Neglecting further the smearing due to finite temperatures as well as any effects caused by internal disorder and inelastic impurity scattering then the sum of transmission probabilities will attain integer values. In this case the conductance will be quantized in units of $\mathrm{G}_0$.

Below we illustrate the quantization of the conductance in a quantum point contact in a simplified picture [10]. Figure 1 shows the conductance quantization as a consequence

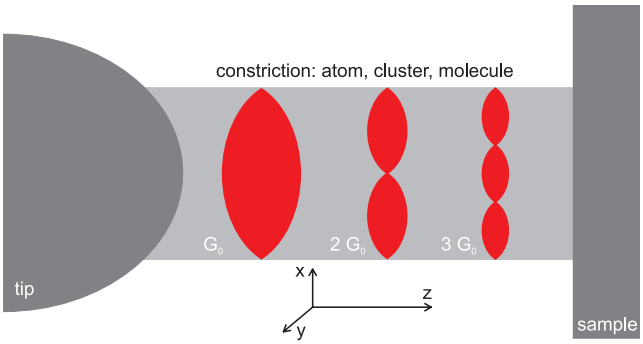


**Figure 1.** Illustration of conductance quantization in an atomic-sized conductor between two electrodes (tip and sample). The electron motion is confined by hard walls at the boundary of the constriction while the potential along the conductor ($z$ direction) is assumed to be flat. The first three eigenmodes are illustrated as standing waves with one, two, three antinodes giving rise to one, two, three conductance channels each contributing a quantum of conductance $\mathrm{G}_0$.

of quantized transverse electron momentum in the contact constriction. Two electrodes which in this case are the tip of a scanning tunnelling microscope (left) and a sample surface (right) are in contact via a constriction provided by a single atom, a cluster of several atoms, or an individual molecule. Assuming that the potential is flat along the conductor ($z$ direction in figure 1) and confines the electron motion in transverse directions ($x$ and $y$ in figure 1), then the electron energy may be written as

$$E = E_i + \frac{\hbar^2 k^2}{2m_e}, \tag{2}$$

where $E_i$ denotes the transverse mode energy, $k$ the wavevector along $z$, and $m_e$ the free electron mass. Coupling this conductor to two reservoirs with potential difference $V$ gives rise to a net current of [11]

$$I_i = e^2 V \varrho_i(E_F)\, v_i(E_F) \tag{3}$$

in the $i$th channel provided that $E_i < E_F$. The density of states ($\varrho_i$) as well as the group velocity ($v_i$) are evaluated at the Fermi energy ($E_F$) since only electrons in a narrow region around this energy contribute to the current. Every mode $i$ accommodates a one-dimensional electron gas with $\varrho_i = 2/(\mathrm{h}\, v_i)$ leading to a total conductance of

$$G = \frac{1}{V} \sum_i I_i = \mathrm{G}_0 \sum_i \Theta(E_F - E_i) = \mathrm{G}_0\, n \tag{4}$$

with $n$ the number of open transverse modes or conductance channels and $\Theta$ the Heaviside step function. In this simple picture, changing the energy of ballistically transferred electrons gives rise to standing waves with $n$ antinodes. Each antinode leads to an additional conductance of $\mathrm{G}_0$. This simplified picture of conductance quantization is in agreement with the above mentioned special case of the multichannel Landauer expression [3, 4, 12–14].

The quantization of conductance was first shown experimentally, in GaAs–AlGaAs heterostructures, by two

groups [15, 16]. In these experiments the width of the point contact was controlled by an applied gate voltage. Upon varying the width of the point contact van Wees *et al* [15] and Wharam *et al* [16] observed a change of the conductance in steps of $G_0$ with intermediate conductance plateaus. Interestingly, Montie *et al* [17] observed the optical analogue of quantized conductance of a point contact. By two-dimensional diffuse illumination of a slit they found a stepwise increase of the transmission cross-section whenever the slit width passed through integer multiples of half of the light wavelength. The diffuse illumination corresponds to the isotropic velocity distribution of incoherent electron waves incident on the point contact.

The first report of a metallic contact of atomic dimension fabricated with the tip of a scanning tunnelling microscope was given by Gimzewski and Möller [18]. Moving an iridium tip towards a thick silver layer adsorbed on Si(111) the authors of [18] observed a sharp transition from tunnelling to contact. Relating the resistance of the tip–surface junction to the Sharvin resistance [2, 19] Gimzewski and Möller concluded that the contact radius was ≈1.5 Å and thus corresponded to the electrical resistance of one or two atoms in close contact. García and Escapa then suggested using a scanning tunnelling microscope to observe oscillatory conductance caused by the confinement of electrons [20]. Experimental data obtained by Pascual and co-workers [21] were interpreted along these lines.

With the development of the mechanically controlled break junction technique [22, 23] conductance steps for niobium and platinum electrodes were reported in 1992 [24]. Striving for an objective data analysis, statistical analysis on a wealth of conductance curves must be performed. Typically, results are presented in the form of histograms [25]. Interestingly, jumps in the integer conductance plateaus were observed and thus distracted from a picture of simply quantized conductance. In fact, these observations inflamed a debate about the origin of conductance steps (see, for instance, [26–28]). A scenario based on mechanical instabilities through which the contact area evolves discontinuously upon breaking or forming the contact could explain conductance steps of the order of $G_0$ even for imperfect conductors [29, 30]. However, this scenario could not account for the pronounced peaks in the conductance histograms at integer multiples of the quantum of conductance. Combination of atomic force microscopy and STM [31, 32] led to the picture of conductance through atomic-sized conductors that we have today: integer values of $G_0$ indicate quantized conductance due to laterally confined quantum modes in the conductor while a jump between the different values is caused by abrupt atomic rearrangements. An extensive review article on quantum properties of atomic-sized conductors as measured mainly by the mechanically controlled break junction technique was given by Agraït *et al* [33]. The reader who is interested in experimental aspects of this technique and in a thorough overview of experimental results and theoretical models is referred to this article.

We notice that table-top experiments performed under ambient conditions likewise revealed conductance quantization. For instance, quantum point contacts were formed by placing two macroscopic metallic wires close to each other and inducing vibrations in the wires by tapping the table top on which the experiment was set up. The wires moved in and out of contact and just before the loss of the contact quantized conductance was observed [34]. A slightly different experimental set-up based on the same idea consisted of hanging a pin very close to a gold plated wafer. Small vibrations cause the pin to go in and out of contact [35]. Hansen and co-workers [36] showed that quantized conductance could also be observed in the breaking contact of commercial electromechanical relays. In a fully automated set-up point contacts were formed and broken several thousand times and the conductance was measured.

A variety of experiments using the tip of a scanning tunnelling microscope to study the conductance of atomic-sized contacts were performed [21, 26, 37, 38]. The main characteristics of these experiments consisted in moving the tip towards the surface, forming and stretching the contact and simultaneously recording the current at a fixed junction voltage. A step forward to more control of the contact junction was provided by the combination of scanning tunnelling microscopes with transmission electron microscopes whose focal point was set at the tip apex. With this technique Ohnishi *et al* [39] were able to relate the quantized conductance through a gold chain directly to the number of gold atoms in the contact. Erts *et al* [40] used a similar approach to study the conductance of gold point contacts as a function of the contact radius. Thus, a direct comparison of the diffusive and ballistic transport regimes was performed and the predictions by Maxwell [1] and Sharvin [2] were verified.

Recent scanning tunnelling microscopy (STM) experiments [41–50] make use of the imaging capability of the instrument with atomic resolution. Contacts to flat surfaces, adsorbed atoms or molecules can therefore be performed controllably and reproducibly without deterioration of either the tip or the sample status. These experiments thus allow one to characterize the electrodes (tip and substrate surface) and the contact constriction (atom or molecule) prior to and after the contact experiment. Therefore, specific atoms or molecular orbitals can be addressed and conductances measured. Because of the detailed characterization of the contact the results of the experiments may serve as precise input for model calculations.

### *1.3. Organization of the review*

In section 2 we expose the experimental set-up. Section 3 describes contacts to flat surfaces (3.1) and to individual adsorbed atoms (adatoms) on surfaces (3.2). Spectroscopy of the differential conductance in contact with a single magnetic atom and the evolution of the Kondo effect from tunnelling to contact is demonstrated (3.3). The contact to adsorbed molecules is the issue of section 4. In this section we discuss conductance curves and their difference with respect to the adatom case (4.1). The dependence of the contact conductance on the molecule orientation, and spectroscopy in contact showing the evolution of molecular orbitals upon contact are addressed (4.2). We close the section about contact to molecules by demonstrating that controlled mechanical contact may induce a reversible change of the molecular orientation (4.3). Section 5 gives a summary and an outlook.

## 2. Experiment

Measurements presented in this article were performed using a custom-made scanning tunnelling microscope operated at 8 K and in ultrahigh vacuum with a base pressure of $10^{-9}$ Pa. Sample surfaces and chemically etched tips were cleaned by argon ion bombardment and annealing. *In vacuo*, the tip was gently indented into the substrate until single adatoms appeared with nearly circular shape in constant-current STM images. As a consequence of this tip preparation we expect the tip apex to be covered with substrate material. Single atoms originating from substrate material were deposited onto the surface by controlled tip–surface contacts as reported in [41] and reviewed in section 3.1. Deposition of cobalt atoms was performed using an electron beam evaporator while $C_{60}$ molecules were sublimed from a heated tantalum crucible. Conductance curves were acquired so as to cover tunnelling to contact regimes. To this end the tip was displaced by 5–6 Å towards the surface and simultaneously the current ranging from the order of 1 nA to the order of 10 $\mu$A was recorded. A linear voltage ramp was applied to the piezo tube carrying the tip leading to advancing and receding velocities of 30–50 Å $s^{-1}$. Zero displacement is defined for a given pair of current and voltage at which the feedback loop is opened prior to conductance measurement. The differential conductance ($dI/dV$) was measured by superimposing a sinusoidal voltage onto the sample voltage (root mean square amplitude between 1 and 5 mV, frequency of 10 kHz) and by detecting the current response with a lock-in amplifier. The junction current is converted to a voltage by a variable gain transimpedance amplifier. Different gains of the amplifier had to be set to measure the current which varied over four orders of magnitude. The input impedances of the amplifier for different gain settings give rise to a voltage drop of less than 0.005% of the applied voltage. Therefore conductances were calculated according to $G = I/V$ with $I$ the current and $V$ the applied voltage. To further rule out possible systematic errors in presented conductance curves we ensured that (i) the relative gain error of the transimpedance amplifier is less than 1% for each applied gain and (ii) the integral nonlinearity for each gain is less than 0.01%.

## 3. Contact to surfaces and adsorbed atoms

### *3.1. Surfaces*

A decrease of the tip–surface distance is related to, for instance, a Stark shift of the binding energy of Shockley-type surface states on noble metal (111) surfaces [51, 52]. For a certain displacement interval the binding energy shifts almost linearly to higher values. Then an accelerated shift sets in which cannot be explained by a junction with constant tip–surface geometry. Rather, due to structural relaxations of the tip as well as of the surface, the distance between tip and surface decreases faster than the tip displacement decreases [51, 52]. Increasing the current further typically leads to a controlled contact between the tip and the surface via a single tip apex atom. This scenario can be monitored by a conductance-versus-displacement curve as shown in figure 2. The conductance

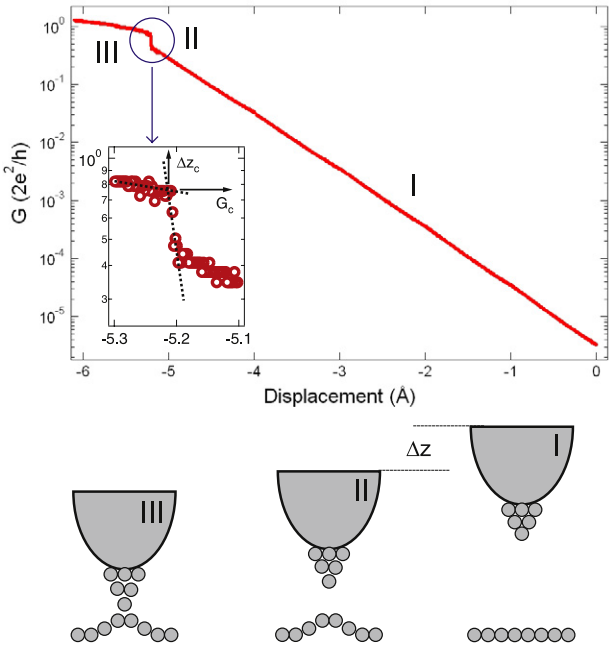


**Figure 2.** Top: conductance-versus-displacement curve acquired on a clean Cu(111) surface at 8 K. Zero displacement corresponds to a tunnelling gap set by feedback loop parameters of 0.1 nA and 0.4 V prior to data acquisition. The conductance is plotted in units of the quantum of conductance on a logarithmic scale. Three regimes are discernible: tunnelling (I), transition (II), and contact (III). Inset: close-up view of transition from tunnelling to contact including the graphical definition of contact conductance ($G_c$) and displacement ($\Delta z_c$). Bottom: illustration of contact formation between tip and flat surface. In the transition regime (II) adhesive forces between the tip and surface lead to relaxations of the tip and surface crystal structure. The tip–surface distance changes not according to the tip displacement $\Delta z$. The contact regime (III) reflects ballistic electron transport through a single atom.

curve is divided into three parts (denoted as I, II, III in figure 2).

In part I the conductance curve appears as a straight line on a logarithmic scale, i.e., the current varies exponentially with the displacement which is characteristic for a tunnelling current. Therefore, part I of the conductance curve is referred to as the tunnelling regime. According to a one-dimensional description of the tunnelling barrier [53] the apparent barrier height may be extracted from

$$\Phi\ [\mathrm{eV}] = 0.952 \left( \frac{\mathrm{d} \ln I}{\mathrm{d}\Delta z\ [\text{Å}]} \right)^2 \qquad (5)$$

where $\Delta z$ denotes the tip displacement (see also the sketch in figure 2). We refer the reader to table 1 which contains a collection of apparent barrier heights obtained for clean surfaces and for single adatoms according to equation (5). Comparing the apparent barrier heights for the clean surfaces with work functions (see third column of table 1) we find reasonable agreement. However, a deviation of the apparent barrier height on the individual adatom by several tenths of an eV with respect to the corresponding surface is observed. This deviation may be related to the dipole moment of the adatom which is induced by charge transfer upon adsorption.

**Table 1.** Apparent barrier height ($\Phi$), work function ($W$), and contact conductance ($G_c$) for various surfaces and adatoms. Error margins for contact conductances correspond to standard deviations obtained by a statistical analysis. Work functions for clean surfaces were taken from [54].

| | $\Phi$ (eV) | $W$ (eV) | $G_c$ ($G_0$) | Reference |
|---|---|---|---|---|
| Ag(111) | 4.0 | 4.74 | $1.5 \pm 0.6$ | Limot *et al* [41] |
| Au(111) | 4.0 | 5.31 | $1.0 \pm 0.4$ | Kröger *et al* [44] |
| Cu(111) | 4.7 | 4.94 | $1.1 \pm 0.3$ | Limot *et al* [41] |
| Ag(111)–Ag | 4.6 | | $0.93 \pm 0.05$ | Limot *et al* [41] |
| Au(111)–Au | 5.0 | | 0.9 | Kröger *et al* [44] |
| Cu(111)–Cu | 5.3 | | $0.98 \pm 0.06$ | Limot *et al* [41] |
| Cu(111)–Co | 4.2 | | 1.0 | Néel *et al* [55] |
| Cu(100)–Co | 3.0 | | 1.0 | Néel *et al* [42] |

Part II of the conductance curve signals an abrupt change of the exponential behaviour. With the time resolution of data acquisition (≈0.1 ms) a discontinuous jump of the conductance is observed (see the inset of figure 2). This part of the conductance-versus-displacement characteristics is referred to as the transition regime since it shows the transition from tunnelling to contact. The conductance right after the jump may be defined as the contact conductance $G_c$ and is, for the particular case of Cu(111) presented in figure 2, given by $G_c \approx 0.8\,G_0$ (see table 1 for a comparison of further contact conductances). We notice, however, that in [41] the contact conductance was defined by the intersection of a linear extrapolation of the tunnelling conductance with the conductance curve in the contact regime. Consequently, contact conductance values taken from [41] are larger than those obtained by the present definition. The tip–surface contact formation exhibited a random character with respect to the contact displacement as well as to the contact conductance (see also the error margins for $G_c$ in table 1). This behaviour can be understood in the light of recent simulations [56]. The jump to contact depends on where the approach is performed on the surface. Regardless of its chemical nature, when the tip is positioned on top of a surface atom the jump should be detected ≈0.5 Å earlier compared to a threefold hollow position case while all other positions lead to a jump to contact within this range. Since surface atoms of compact (111) surfaces are not usually resolved the conductance measurements were performed at random locations of the surface and the jumps occur randomly within a finite displacement interval of the tip around 0.5 Å which is in agreement with the above simulation. Therefore contact conductances obtained for flat surfaces usually exhibit larger standard deviations (≈0.5 $G_0$ [41]) than those obtained for single adatoms (≈0.05 $G_0$ [41]).

In the contact regime (part III) the conductance of the tip–surface junction varies slowly with tip displacement. Retracting the tip after this discontinuous jump and imaging the contacted surface area in ≈70–80% of the cases a single adatom was found. This observation together with simulations [41] put forward a scenario where tip and surface are connected via a single atom during contact.

Why is a jump to contact observed? The jump occurs when chemical bonds between the surface and the tip apex start to weaken the adhesion of the atom to the tip structure. In this case and over a relatively small distance variation of less than 0.1 Å the atom will be transferred from the tip to the surface. We notice in this context that from continuum models and atomistic simulations an attractive force between two clean metal surfaces was predicted which leads to an intrinsic instability at a distance of 1–3 Å and causes the surfaces to snap together on a timescale of the order of 100 fs [57, 58].

In all cases we observed a contact conductance close to $G_0$ which together with the observation of a single adatom after contact is evidence for a single-atom contact. Monovalent atoms like Ag, Au, and Cu are expected to provide a single channel for electron transport [59]. In particular, the transmission probability for a single-Au-atom contact was calculated to give ≈1 for the $sp_z$ orbital which exhibits the highest density of states at the Fermi level [60].

### 3.2. Adatoms

The controlled contact to individual adsorbed atoms using the tip of a scanning tunnelling microscope was first investigated by Yazdani *et al* [61]. The conductance of individual xenon atoms adsorbed on a nickel surface was studied using a bare tungsten tip and a tip terminated by a xenon atom. Contact conductances of ≈0.2 $G_0$ and of ≈0.001 $G_0$ were reported for the single xenon atom and the two-atom chain, respectively. In particular, no jump to contact was observed. In [10] contact experiments were reported for single Mn and Gd atoms adsorbed on a Cu(100) surface. A clean Au tip was used to contact these atoms giving rise to contact conductances of $(0.87 \pm 0.07)\,G_0$ and $(0.52 \pm 0.10)\,G_0$ for Mn and Gd atoms, respectively. A contact junction consisting of two Mn atoms bridging the gold tip and the copper surface was fabricated by contacting an adsorbed Mn atom with a Mn-terminated Au tip. The resulting contact conductance was $(0.95 \pm 0.04)\,G_0$ [10]. All conductance-versus-displacement curves exhibited a smooth transition from tunnelling to contact rather than a jump to contact.

Contact to metallic adatoms using the tip of a scanning tunnelling microscope was then reported by Limot *et al* [41], Néel *et al* [42, 45], and Kröger *et al* [44]. In accordance with contact experiments reported by Yazdani *et al* [61] and Bürgi [10] no discontinuous transition from tunnelling to contact was observed. Rather, for the adatoms investigated, i.e., Ag on Ag(111) and Cu on Cu(111) [41], Co on Cu(100) [42, 45], and Au on Au(111) [44], a continuous transition takes place. Additionally, in contrast to the tip–surface contact case, no material is transferred to the surface. Moreover, the tip–adatom contact does not exhibit the random character as observed for the tip–surface contact (see also the significantly lower standard deviation of $G_c$ in table 1). In figure 3 we present a conductance curve for Cu(111)–Cu. Similar to the tip–surface junction case three regions of the conductance characteristics are discernible. In the tunnelling regime the current varies exponentially with the displacement giving rise to an apparent barrier height which is larger by a few tenths of an eV than that observed for the clean surface. As a marked difference the transition between

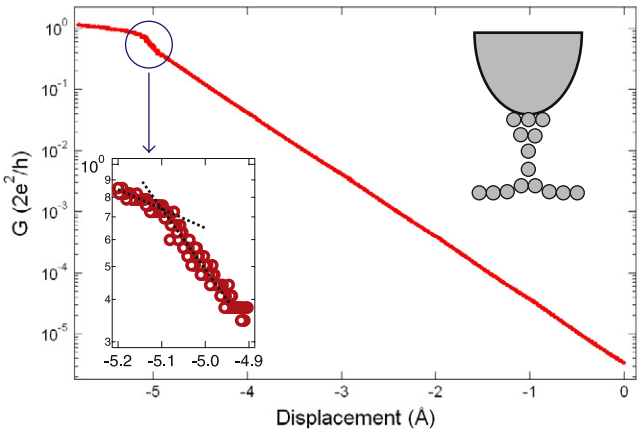


**Figure 3.** Conductance–displacement characteristics of a single adsorbed Cu atom on a Cu(111) surface acquired at 8 K. Zero displacement corresponds to a tunnelling gap set by feedback loop parameters of 0.1 nA and 0.4 V prior to data acquisition. Lower inset: close-up view of the transition between the tunnelling and contact regime. Upper inset: illustration of the tip–adatom contact.

tunnelling and contact is now continuous at the time resolution of data acquisition (see the inset of figure 3). The reason for this difference is the larger stiffness of the adatom bond to the surface. An increase of the elastic constants by ≈100% compared to those for flat surfaces was found [41, 62]. This indicates that the redistribution of surface charge due to the Smoluchowski effect creates a surface dipole which enhances the bonding of the adatom. The dipole moment of the adatom is in agreement with the increased barrier height inferred from the slope of the conductance curve. It was shown in [41] that the tip–adatom interaction remains well below the threshold value necessary for the jump to contact observed on flat surfaces.

Noble metal atoms are monovalent and are thus expected to exhibit a single conductance channel. If the transmission probability equals 1 then the contact conductance should be exactly $1\,G_0$. There are possible reasons why the ideal contact conductance of a monovalent atom is not observed in the experiment. Equation (1) gives the contact conductance as a sum over conductance channels which exhibit a certain transmission probability. In the case of a monovalent atom equation (1) simply reads $G = \tau\,G_0$. A deviation of the conductance from $1\,G_0$ may therefore be related to a deviation of the transmission probability $\tau$ from 1. In fact, the transmission probability for a given atomic conductance channel depends on the connection of the atom to neighbouring atoms in the metallic leads. Only in the absence of defects in the leads close to the central atom and in the absence of excitations of other degrees of freedom would we measure a transmission probability of 1. Any partial reflection of the electron wave as a result of, for instance, the mismatch of the waves on either side of the constriction may alter the current and thus the conductance. Therefore, scattering centres near the contact give rise to a number of corrections, the most obvious of which is a reduction of the total conductance.

The conductance of a single Co atom adsorbed on Cu(100) was determined to be $1.03\,G_0$ [42]. According to [59], transition metals give rise to five conductance channels. Thus, completely open channels would lead to a contact conductance of $5\,G_0$, rather than $\approx 1\,G_0$ as observed for the Co atom. Assuming that all channels contribute equally to the total conductance each conduction channel would exhibit a transmission probability of ≈0.2. Using the mechanically controlled break junction technique [59, 63] Nb atomic contacts were investigated yielding conductances between 1.5 and $2.5\,G_0$. Here five conduction channels with transmission probabilities ranging from ≈0.02 to ≈0.73 were reported.

### *3.3. Spectroscopy in contact*

We adhere to the study of magnetic adatoms on metal surfaces and in contact with a STM tip and show that contact modifies the spectroscopic signature of the Kondo effect. The preceding part showed that controlled and reproducible contact to individual adsorbed atoms on surfaces is feasible with the tip of a scanning tunnelling microscope. In a next step the obvious question of whether the contact junction is stable enough to enable spectroscopy was addressed [42]. To this end spectroscopy was performed on magnetic atoms which owing to the Kondo effect exhibit a characteristic resonance close to the Fermi level in tunnelling spectra of $\mathrm{d}I/\mathrm{d}V$ [64, 65].

Figure 4(a) shows the conductance–displacement characteristics of a single Co adatom on Cu(100) [42, 45]. The arrows indicate the conductances at which the feedback loop was opened for the measurement of $\mathrm{d}I/\mathrm{d}V$. Spectra in the tunnelling (A) as well as in the contact (B) regime are displayed in figure 4(b). Around zero sample voltage we find the spectroscopic signature of the Kondo effect [64–67]. A modified resonance is likewise observed in the contact regime (see spectrum B in figure 4(b)). However, an apparent broadening of the line shape is obvious. To quantify this broadening a variety of spectra acquired in the tunnelling as well as in the contact regime were described by a Fano line shape according to

$$\frac{\mathrm{d}I}{\mathrm{d}V} \propto \frac{(q+\epsilon)^2}{1+\epsilon^2} \tag{6}$$

with $\epsilon = (eV - \epsilon_K)/(k_B T_K)$ ($\epsilon_K$: resonance energy, $k_B$: Boltzmann's constant) and $q$ the asymmetry parameter of the Fano theory [68]. The additional width of the resonance is then reflected by an increased Kondo temperature. We notice that extracted values of $T_K$ depend to some extent on the voltage interval chosen for the fit. Figure 5 compares experimentally determined (triangles) and calculated (circles) Kondo temperatures as a function of the tip displacement. An abrupt change of $T_K$ at a displacement of $\Delta z \approx -4.1$ Å is observed in both data sets. For displacements $\Delta z > -4.1$ Å experimental as well as theoretical Kondo temperatures vary between 70 and 100 K. In the contact regime ($\Delta z < -4.1$ Å) experimental Kondo temperatures vary between 140 and 160 K while theoretical results scatter within 200 and 290 K. The abrupt broadening of the Fano resonance upon contact was therefore interpreted as reflecting a sudden increase of $T_K$ [42].

On the basis of density functional theory and on the concept of an Anderson impurity [69, 70] the change of $T_K$ was traced back to a shift of the Co d band towards the Fermi level [42]. Additionally, a broadening of the band due to

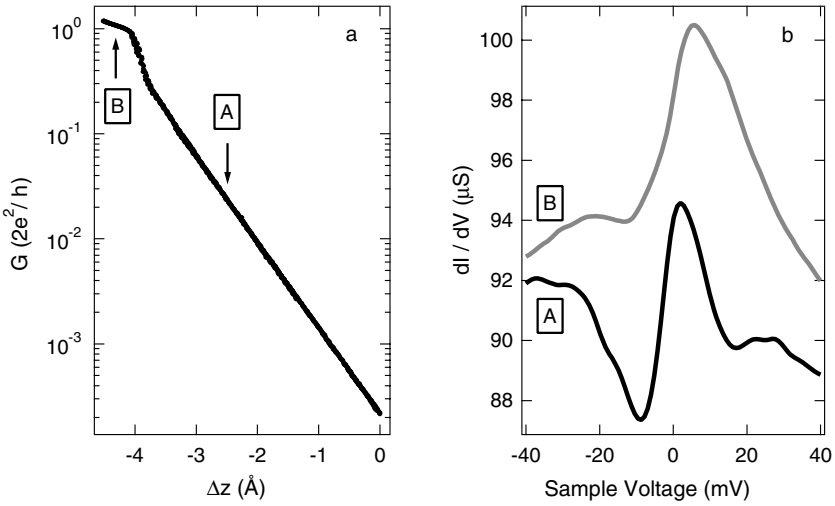


**Figure 4.** (a) Conductance–displacement characteristics of a single adsorbed Co atom on a Cu(100) surface acquired at 8 K. Zero displacement corresponds to feedback loop parameters of 1 nA and 0.06 V. (b) Spectra of differential conductance ($\mathrm{d}I/\mathrm{d}V$) recorded in the tunnelling (A) and the contact (B) regime indicated in (a). The spectra show a Fano resonance at the Fermi energy ($V = 0$ V) induced by the Kondo effect.

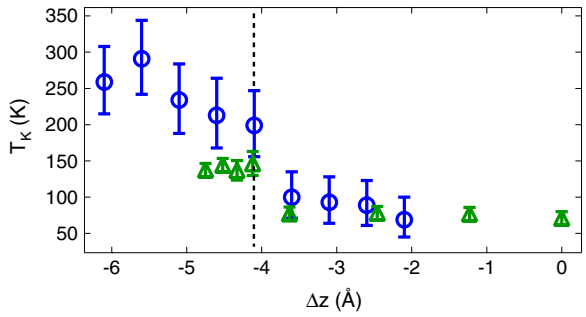


**Figure 5.** Experimental (triangles) and calculated (circles) Kondo temperatures ($T_K$) as a function of the tip displacement. The dashed line at $\approx -4.1$ Å indicates the transition from tunnelling ($\Delta z > -4.1$ Å) to contact ($\Delta z < -4.1$ Å).

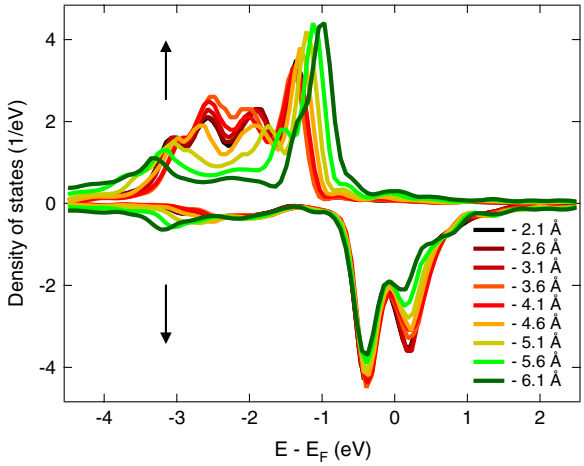


**Figure 6.** Density of states (DOS) depending on the tip displacement. Spin-up (↑) and spin-down (↓) DOS are plotted as positive and negative values, respectively. The d ↑ band is shifted toward the Fermi energy with decreasing displacement.

an increased coordination number of the magnetic impurity was inferred. Figure 6 illustrates the main theoretical results. Here, the spin-polarized density of d states at the position of the Co adatom is shown. During a tip approach the main changes occur in the spin-up band of cobalt. The closer proximity of the tip induces a shift of the band towards the Fermi level and a broadening of individual peaks. A similar scenario was found in [71]. Since the width of the d level is a measure for the hybridization with conduction electrons of the Cu substrate and the tip, it is plausible that the width increases with decreasing tip–adatom distance. Deviations of calculated Kondo temperatures from experimentally determined values in the contact regime may be due to the simple model applied. In particular, the Fano line shape might be no longer appropriate for the contact regime and improved models may have to be involved to extract a more precise Kondo temperature from experimental data. However, it must be emphasized that absolute values of $T_K$ in the tunnelling regime as well as the significant change of $T_K$ at the transition from tunnelling to contact are well accounted for in the simulations.

## 4. Contact to single adsorbed molecules

### *4.1. Conductance and local heating of a $C_{60}$ molecule*

To the best of our knowledge the first STM experiment addressing a tip–molecule contact was reported by Joachim *et al* [72] for $C_{60}$ adsorbed on Au(110). In this pioneering work Joachim *et al* studied the conductance of the tip–molecule junction as a function of the tip displacement at room temperature. Below we review the results of more recent experiments [43, 45, 46, 49, 50] addressing the controlled contact to a $C_{60}$ molecule on Cu(100) at low temperatures.

Figure 7(a) shows an STM image of Cu(100)–$C_{60}$ in a submonolayer coverage regime. The bright and dim rows correspond to chains of $C_{60}$ molecules along the indicated crystallographic directions. Combining STM and x-ray

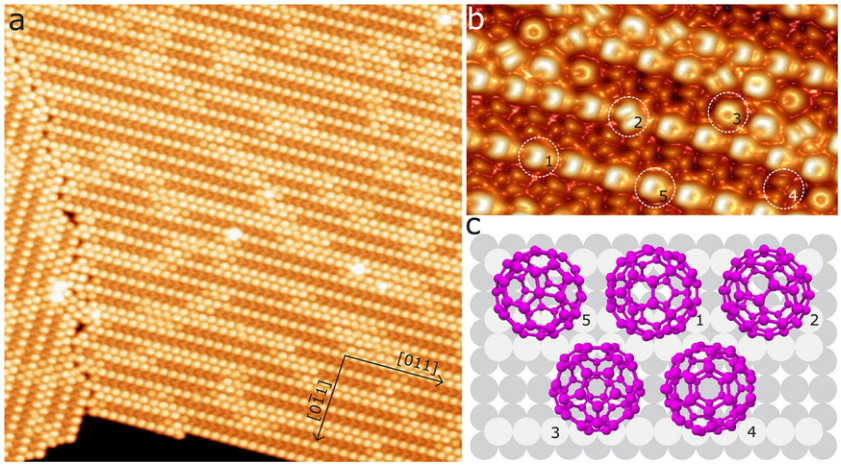


**Figure 7.** (a) STM image of a $C_{60}$ island adsorbed on Cu(100) ($V = 1.5$ V, $I = 1$ nA, 400 Å × 400 Å, $T = 8$ K). Molecule chains appear as bright and dim rows due to adsorption-induced surface missing-row reconstruction. (b) Close-up view of (a) showing individual $C_{60}$ molecules with intramolecular structure (130 Å × 75 Å). (c) Molecule orientations **1**–**5** indicated in (b) by dashed circles on missing-row reconstructed Cu(100). Bright (dark) circles correspond to topmost (second) Cu layers. Molecules with orientations **1**, **2**, **5** reside on a single missing row while molecules with orientations **3**, **4** are adsorbed in a double missing row.

photoelectron diffraction data Abel *et al* [73] concluded that these stripe patterns were due to a $C_{60}$-induced missing-row reconstruction of the underlying substrate surface. The close-up view in figure 7(b) displays individual $C_{60}$ molecules within the bright and dim stripes with submolecular resolution. We attribute this pattern exposed to vacuum to the spatial distribution of the local density of states of the second-to-lowest unoccupied molecular orbital (LUMO+1) in agreement with [74, 75]. Figure 7(c) identifies the adsorption geometry of $C_{60}$ molecules encircled by dashed lines in figure 7(b). Molecules **1**, **2**, and **5** adsorb on a single missing row of the Cu(100) surface while molecules **3** and **4** reside in a double missing row. The orientations of the molecules differ, i.e., molecule **1** exhibits a carbon–carbon bond between a pentagon and a hexagon at the top, molecule **2** shows a carbon–carbon bond between two adjacent carbon hexagons, molecules **3** and **4** expose a pentagon and a hexagon at the top, respectively, while molecules with orientation **5** exhibit a carbon atom at the top. In this part we focus the discussion on molecules of type **1**.

How does the conductance of an individual molecule change with decreasing distance between the tip and the molecule? Figure 8 shows the conductance–displacement characteristics of molecules with orientation **1**. The conductance curve for the single molecule bears a resemblance to the conductance curve of a single adatom. In particular, a continuous transition between tunnelling and contact is again observed. A marked difference, however, concerns the contact conductance which is only $\approx 0.25\,G_0$. Figure 8 contains calculated data depicted as squares. A detailed description of the applied model can be found in [43]. The most intriguing observation is that theory is able to model the sharp increase of the conductance as well as a contact conductance below $G_0$. The rapid rise of the conductance in the displacement interval between $\approx -1.6$ Å and $\approx -2.0$ Å can be understood from the relaxed tip–molecule geometries which the model calculations are based on. As the electrode separation is reduced by only

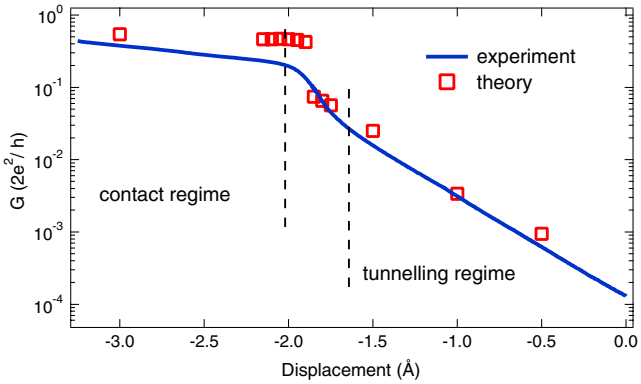


**Figure 8.** Conductance-versus-displacement curve for a $C_{60}$ molecule adsorbed on Cu(100) with orientation **1**. Owing to the high number of data points, experimental data appear as a line. Calculated data are depicted as squares. Zero displacement corresponds to a tip–molecule distance defined by feedback loop parameters of 3 nA and 0.3 V.

0.05 Å the tip–molecule distance decreases by 0.84 Å. This strong reduction of the tip–molecule distance corresponds to the formation of a bond between the tip apex and the $C_{60}$ which hence effectively closes the tunnelling gap.

In this transition regime, between tunnelling and contact, only small energy differences discriminate between the configurations with and without the tip–molecule bonds [42]. At finite voltages and under nonequilibrium conditions imposed by the bias voltage it is thus likely that the junction will fluctuate between these different configurations. With $G_t$ and $G_c$ the conductances just before and just after the contact, respectively, a thermally averaged conductance can be calculated according to

$$\bar{G}(\Delta z) = \frac{G_t(\Delta z)\exp(-\beta E_t(\Delta z)) + G_c(\Delta z)\exp(-\beta E_c(\Delta z))}{\exp(-\beta E_t(\Delta z)) + \exp(-\beta E_c(\Delta z))} \quad (7)$$

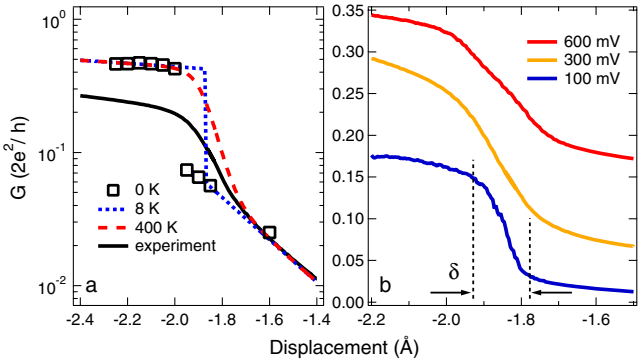


**Figure 9.** (a) Width of the transition regime dependent on the effective temperature of the junction. Experimental data taken at 8 K appear as a line while calculated data are depicted as squares for $T_{\mathrm{eff}} = 0$ K, as a thin dashed line for $T_{\mathrm{eff}} = 8$ K, and as a thick dashed line for $T_{\mathrm{eff}} = 400$ K. (b) Comparison of conductance curves acquired at indicated voltages. The width, $\delta$, of the displacement interval for the transition is shown for the curve taken at 100 mV. Conductance curves at 300 and 600 mV are vertically offset.

with $\beta = (k_B T)^{-1}$. $E_t$ and $E_c$ denote the total energies of a tunnelling and a contact configuration, respectively. In figure 9 we focus on the conductance curve in a displacement interval around the instability point. Increasing the effective temperature of the tip–molecule junction from 0 K (squares in figure 9(a)) via 8 K (thin dashed line) up to 400 K (thick dashed line) leads, first, to an increase of the width of the transition regime and, second, to a shift of the instability displacement to more positive values. At an effective temperature of 400 K the width of the calculated conductance curve matches well the width of the experimental curve. Because of this elevated temperature we propose a scenario of local heating of the molecule in contact with the tip. This suggestion is further corroborated by the experimental observation of a voltage-dependent width of the transition regime (see figure 9(b)). In table 2 we compare the widths of the transition regime and the corresponding effective temperatures according to equation (7).

The dependence of the effective temperature on the voltage was modelled for atomic-sized contacts by assuming a bulk thermal conduction mechanism [76–78]. From these investigations it follows that the effective temperature for low ambient temperatures is proportional to the square root of the voltage. However, there are examples where the effective temperature rises more rapidly than $\sqrt{V}$, for instance, in the case of bias-induced local heating of Zn atomic-sized contacts [79]. For octanedithiol the $\sqrt{V}$ law for the effective temperatures seems to approximately hold [80] while in our case of $C_{60}$ more experimental data and theoretical analysis would be needed to estimate the voltage dependence of the effective temperature.

The first experiment using the mechanically controlled break junction technique to investigate single-molecule conductance was reported in 1997 [81]. Gold electrodes were allowed to interact with a solution of benzene-1,4-dithiol forming a self-assembled monolayer on the electrodes. The junction was then closed and opened a number of times and

**Table 2.** Widths of the transition interval ($\delta$) and effective temperatures ($T_{\mathrm{eff}}$) for conductance curves acquired at different voltages ($V$).

| $V$ (mV) | $\delta$ (Å) | $T_{\mathrm{eff}}$ (K) |
|---|---|---|
| 100 | 0.2 | 300 |
| 300 | 0.4 | 400 |
| 600 | 0.5 | 700 |

current–voltage characteristics were recorded at a position just before the contact was lost. A fairly large energy gap of 2 eV was attributed to a metal–molecule–metal junction. Further similar experiments were performed by Kuergeris *et al* [82] and Reichert *et al* [83, 84]. Smit *et al* [85] observed that while a clean Pt single-atom contact exhibited a conductance of $(1.5 \pm 0.2)\,G_0$, hydrogen-covered electrodes lead to a conductance peak near $1\,G_0$. To date the molecular arrangement responsible for the conductance of $1\,G_0$ is unclear. In a recent work by Böhler *et al* [86] a mechanical break junction with gold electrodes was used to measure the conductance of adsorbed $C_{60}$ molecules. Inferring the presence of the molecule from characteristic vibrational spectra, a somewhat smaller contact conductance of $0.1\,G_0$ was reported.

In the next part, contact experiments on differently oriented $C_{60}$ molecules using the tip of a scanning tunnelling microscope are introduced. These experiments owing to imaging the molecules prior to and after conductance measurements provide precise information about the contact geometry.

### *4.2. Conductance of oriented molecular orbitals*

Recent work demonstrated that molecular conformations [87–91] and orientations [48] affect the conductance. Despite this progress, the atomic arrangement at the molecule–metal interface usually remains unknown. Theoretical work, for instance [92, 93] and references therein, as well as experiments on metallic single-atom contacts [33, 94], however, highlight the importance of the details of this interface. Therefore, an ideal experiment would allow one to address specifically the object to be contacted. As a consequence, the contact geometry would be unambiguously determined and may find its way into calculations which otherwise would have to assume the contact configuration. In this part we review the results obtained for a prototypical molecular contact of a single $C_{60}$ molecule attached to Cu contacts in different orientations [48]. A remarkable influence of the contact geometry on the individual molecule conductances is found. We concentrate on the contact conductances of molecules with orientations **1**–**4** introduced in the preceding part (see figure 7).

While conductance curves for all $C_{60}$ orientations exhibit the same general characteristics as were discussed for molecule **1** in the preceding part, there are marked and important differences to be discussed next. Since these differences concern the transition and contact regimes, figure 10(a) focuses on conductance curves of the four $C_{60}$ species in the corresponding displacement interval. In particular, only a small fraction of the tunnelling regime is visible for molecule **3**.

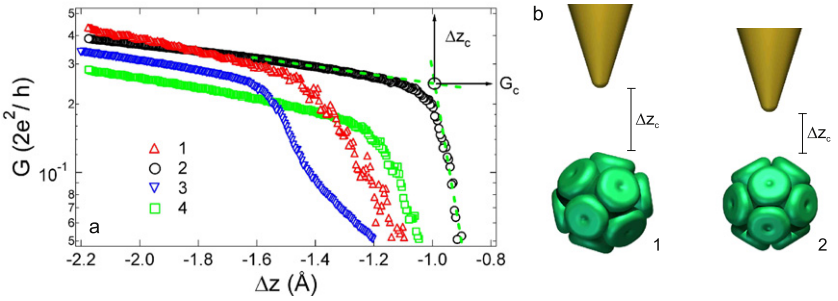


**Figure 10.** (a) Conductance curves of $C_{60}$ orientations **1**–**4** in the transition and contact regimes. Dashed lines indicate the graphical definition of contact displacement and conductance. Zero displacement is defined by feedback loop parameters of 1 $\mu$A and 0.4 V. (b) Sketch of tip and molecule **1** (left) and **2** (right) prior to opening the feedback loop for conductance measurement. Since the density of states of the LUMO is higher at the tip for molecule **1** the tip excursion for reaching contact is higher than in the case of molecule **2**.

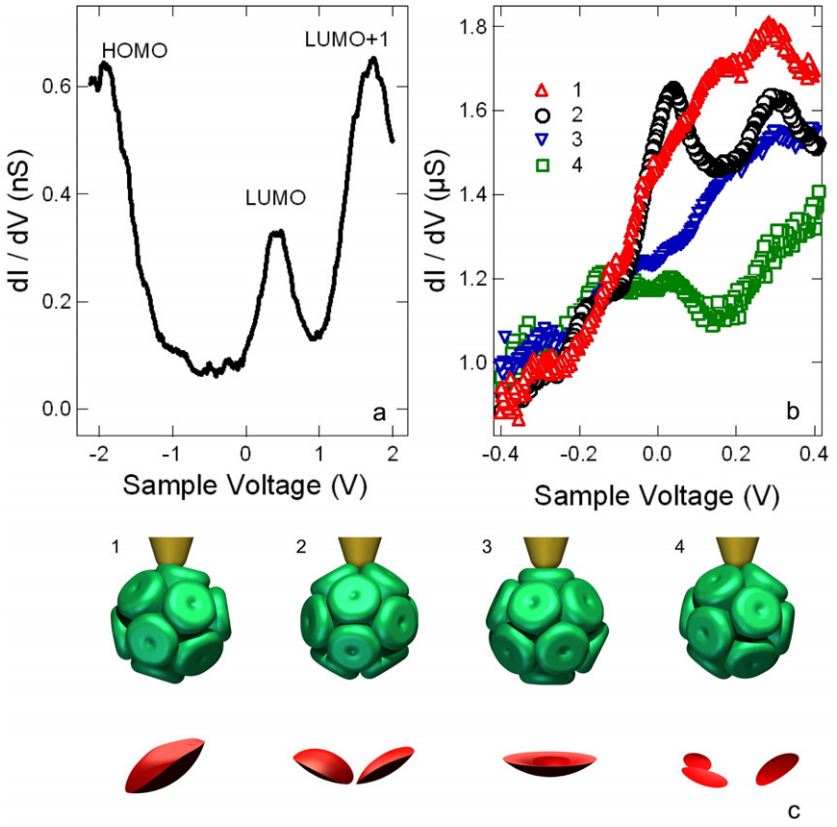


**Figure 11.** (a) Spectrum of the differential conductance ($dI/dV$) acquired on a single $C_{60}$ molecule at 8 K in the tunnelling regime. The spectrum is fairly insensitive to the molecular orientation. Peaks are attributed to highest occupied molecular orbital (HOMO), lowest unoccupied molecular orbital (LUMO) and the second-to-lowest molecular orbitals (LUMO + 1). (b) $dI/dV$ spectra at contact for the different molecular orientations. For comparison, spectra were normalized to conductance at $-0.4$ V. (c) Top row: illustration of tip contact to molecules **1**–**4**. Molecules are identified via characteristic orientation of the LUMO. Bottom row: intersection of a spherical Cu 4s orbital with the toroidal LUMO at 5.4 Å distance. Volumes decrease from left to right in the sequence 100:57:33:8.

Two results are obvious: (i) the displacements for contact formation ($\Delta z_c$) as well as (ii) the contact conductances ($G_c$) differ for the molecule orientations. We notice that conductance values depend on the tip shape. Blunt tips giving rise to STM images of $C_{60}$ without submolecular resolution typically resulted in contact conductance values of ≈0.5–0.7 $G_0$. To obtain reproducible conductance curves as shown in figure 10 the tip had to be prepared *in vacuo* so as to give sharp STM images with submolecular resolution.

The different contact displacement may be explained by the spatial extension of the lowest unoccupied molecular orbital (LUMO) into vacuum. The conductance curves shown in figure 10(a) were acquired after opening the feedback loop at a voltage of 0.4 V. At this voltage electrons can tunnel resonantly into the LUMO (see figure 11(a)). Depending on the local density of states of the LUMO with specific orientation probed by the tip the tip–molecule distances differ. As a consequence the tip starts its trajectory towards the molecule

**Table 3.** Comparison of contact displacements $\Delta z_c$ and conductances $G_c$ of molecules exhibiting orientations **1**–**4**.

| Orientation | $\Delta z_c$ (Å) | $G_c$ ($G_0$) |
|---|---|---|
| **1** | −1.39 | 0.26 |
| **2** | −0.98 | 0.25 |
| **3** | −1.57 | 0.26 |
| **4** | −1.18 | 0.17 |

at different heights above the molecule and therefore must be displaced differently until contact is formed (see figure 10(b) for an illustration). The differences in contact displacements (see table 3) agree very well with differences in apparent heights inferred from constant-current STM images acquired at 0.4 V (not shown).

The second marked difference of the conductance curves concerns the contact conductances. While contact conductances of molecules with orientations **1**–**3** are similar, molecules with orientation **4** with a hexagon pointing towards the tip clearly are less conducting (see table 3 for a comparison). We therefore conclude that electron transport through the same molecule depends crucially on the orientation that the molecule adopts, between the contacting electrodes. Our observation that contact conductances differ for all $C_{60}$ orientations (and are below 1 $G_0$) may be related to the number of transport channels and their transmission probability. Preliminary calculations reveal that the main transport channel of the tip is provided by the 4s orbital of the Cu tip apex atom while the secondary channel given by the 4p orbital is conducting an order of magnitude less. For $C_{60}$ due to a lack of calculations we assume that the LUMO contributes considerably to electron transport through the molecule. To test the validity of this assumption to some extent we performed additional investigations.

First, we looked for the energy of the LUMO in a spectrum of $\mathrm{d}I/\mathrm{d}V$ acquired in the tunnelling regime above a $C_{60}$ molecule (figure 11(a)). At a sample voltage of 0.4 V—at which the conductance curves presented in figure 10(a) were acquired—the spectrum is dominated by the spectral signature of the LUMO. Peaks related to the highest occupied molecular orbital (HOMO) and the LUMO +1 contribute to the spectrum at widely different energies. We notice that these assignments of peaks in $\mathrm{d}I/\mathrm{d}V$ spectra to molecular orbitals are based not on calculations but on a qualitative comparison with findings reported for the similar system Ag(100)–$C_{60}$ [75]. In the tunnelling regime these spectra are similar for all molecule orientations. *A priori*, it is not at all clear that the molecular orbitals remain unchanged at contact. For instance, previous work on metal contacts has revealed Stark shifts of electronic states [51, 52]. Therefore, secondly, we recorded spectra of the differential conductance at contact. The molecular junctions are stable enough to enable this type of measurement. Figure 11(b) presents the results. While $\mathrm{d}I/\mathrm{d}V$ spectra in the tunnelling regime vary little even at elevated currents, significantly altered characteristics are observed at contact. For instance, molecule **1** exhibits a steady increase of its $\mathrm{d}I/\mathrm{d}V$ signal while molecule **4** shows an almost flat $\mathrm{d}I/\mathrm{d}V$ curve. From these spectra we infer that the signature of the LUMO is still present for all molecules but is significantly modified depending on the molecular orientation. In figure 11(c) we combine the available information and estimate the overlap of the Cu 4s orbital at the tip apex with the $C_{60}$ LUMO for the different orientations by calculating their volume of intersection. For the Cu 4s orbital we assumed a sphere with a diameter of 2.5 Å which corresponds to the nearest-neighbour distance in the copper crystal. For the LUMO we assumed a toroidal shape as reported in [75]. We further assumed a distance between the centre of the spherical Cu 4s orbital and the centre of the $C_{60}$ cage of 5.4 Å. This contact distance relies on calculations performed in [43]. As an approximation we applied the same contact distance for all molecules. Within this simplified picture of tip–molecule contact (see the top row of figure 11(c)) we calculated the volume of intersection between the Cu 4s and the toroidal molecule orbital (see the bottom row of figure 11(c)) and took it as a measure for the degree of overlap. Consistent with experimentally measured $G_c$, the overlap between the tip and molecule orbital is largest for type **1** and smallest for type **4**. While yielding a correct sequence of conductances, the model is clearly too simple for reliable predictions. Nevertheless, it provides further indication of the relevance of conductance through the LUMO.

### *4.3. Orientation change in a single-molecule contact*

In this part we report on a controlled and reversible change of $C_{60}$ adsorption orientations on Cu(100) when the molecule is in contact with the STM tip [47]. Currently, considerable attention is devoted to employing small ensembles or even individual atoms or molecules as building blocks in electronic circuits. For instance, bistable switches were realized by the motion of single xenon atoms between the tip of a scanning tunnelling microscope and a nickel surface [95], by reversibly switching between two stable orientational configurations [96], and by conformational changes of molecules induced by tunnelling electrons [88, 97–99] or photons [100]. Further examples are the regulation of single-molecule conductivity by an electrostatic field [101], the direct modification of dynamical properties of an individual molecule by single-atom manipulation [90], and the control of a complex sequence of coupled rotational and translational dynamics by rolling of a single $C_{60}$ molecule on a silicon surface [102]. Despite these pioneering works the specific addressing of individual molecules to modify reversibly mechanical or electronic properties remains scarce. In particular, experiments providing control of the contact geometry as well as of the contacting electrodes may give complementary information to the widely used mechanically controlled break junction technique.

For the study of a controlled and reversible switch of a $C_{60}$ adsorption orientation we additionally consider the fifth molecule type which has already been introduced in section 4.1. The rotation of the $C_{60}$ molecule occurs during contact with the tip. We observed that displacing the tip beyond a threshold excursion can cause the molecule to rotate. The threshold is located at displacements in regime III where the conductance starts to increase again. In this region, in particular for displacements larger than the threshold,

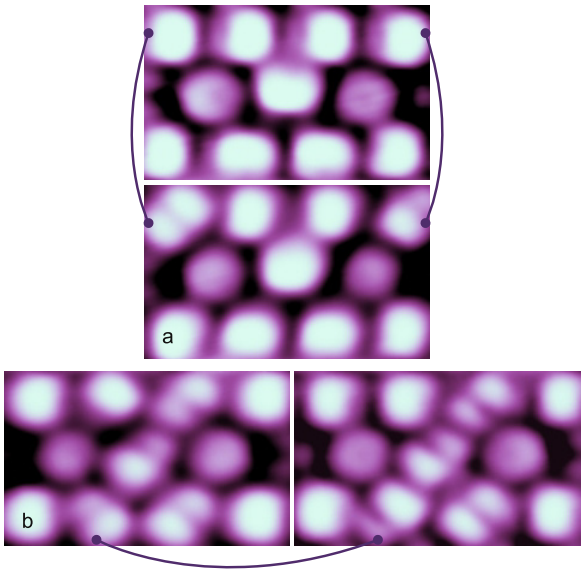


**Figure 12.** STM images of the same surface area of Cu(100) covered with a single layer of $C_{60}$ ($V = 1.7$ V, $I = 0.1$ nA, 35 Å × 20 Å, $T = 8$ K). (a) Orientation change of molecules in contact with the tip. Top: prior to contact indicated molecules exhibit orientation **1**. Bottom: after contact indicated molecules are in orientation **2**. (b) Apparent in-plane rotation of molecule type **1** by 90°.

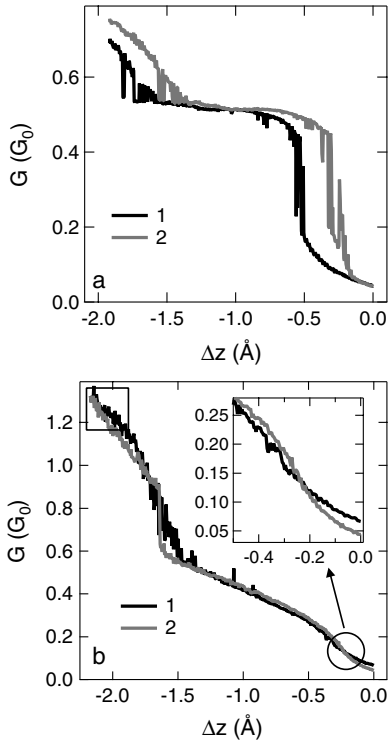


**Figure 13.** (a) Single conductance-versus-displacement curve of molecule **1** (black) together with single conductance–displacement characteristics of a molecule with orientation **2** (grey). The black curve was acquired prior to and the grey curve just after rotation. (b) Conductance curves acquired during tip approach to (grey) and tip retraction from (black) a $C_{60}$ molecule. During the tip displacement the molecule changed from **2** to **1**, most probably at a tip displacement exceeding −2.1 Å where conductance curves coincide (square). Feedback loop settings prior to data acquisition: 1 $\mu$A, 0.3 mV. Inset: close-up view of conductance traces close to zero tip displacement showing a conductance difference of ≈0.02 $G_0$ which is related to a different apparent height of the molecules.

reproducibility of the measurements strongly depends on the tip shape as well as on the position of the contact over the molecule. Different slopes and shapes of this conductance rise were observed. However, for all measurements this continuous rise was observed to lead to a—on the 100 $\mu$s timescale of data acquisition—discontinuous jump of the conductance at higher tip displacements. The discontinuous jump of the conductance may be attributed to a modified geometry of the contact atomic structure [43]. It is reasonable to assume that during the continuous rise of the conductance preceding the rearrangement of the contact atomic structure the molecule adsorption geometry is already slightly modified. Once the tip is retracted the molecule returns to one of its stable configurations. The rotation occurred when this final configuration differed from the initial one before the contact with the tip.

Rotations of the molecule are illustrated by the STM images of figure 12. The indicated molecules in figure 12 were contacted by the tip of the microscope, and on increasing the tip displacement above a threshold the molecules switched from one molecule type to the other (figure 12, from **1** to **2**) or performed an apparent in-plane rotation (figure 12). A variety of rotation experiments revealed that rotation of **2** and **5** molecules always leads to **1** molecules, while rotating **1** molecules leads to **2** or **5** species. A configuration change from species **1**, **2**, **5** to **3**, **4** or vice versa, however, has never been observed. Moreover, contact between the tip and a molecule residing in the double missing row (**3** or **4**) did not lead to a modification of the molecule adsorption configuration. Modifying the tip apex shape by indentation of the tip into the substrate surface led to the same observation, indicating that this phenomenon is rather tip independent.

As shown in the previous part, the adsorption configuration of the $C_{60}$ molecule directly determines the conductance characteristics. In particular, given that feedback loop parameters are the same prior to performing contact measurements, the contact displacement of the tip is different for molecules **1**–**5**. Here we restrict the discussion to **1** and **2** orientations. It is possible to observe the rotation via the conductance–displacement characteristics as illustrated in figure 13. The single (non-averaged) conductance curves are assigned to a molecule with orientation **1** (black) and **2** (grey). The black curve was acquired just before an orientation switch while the grey curve was taken directly after. Both curves exhibit fluctuations in the transition region as well as in the contact region when the conductance starts to rise again. Fluctuations in the transition region have been interpreted in terms of local heating of the molecule (see [43, 45, 46, 50] and section 4.1). These fluctuations do not lead to rotation of the molecule. Displacing the tip beyond excursions where the conductance rises again, however, can cause the molecule to rotate. Thus, a threshold excursion of the tip must be reached before a change of the adsorption configuration occurs [43].

To investigate the probability of switching for different tip displacements we used the fact that the conductance curve

is characteristic of the adsorption configuration. For each value of the displacement with the same initial conditions 500 conductance measurements were performed and the number of switching events was counted. The switching probability rises sharply above a threshold displacement of ≈−1.9 Å to ≈30% rather independently of the tip displacement.

To explore whether hysteresis-like effects may be observable, in figure 13(b) we present a conductance curve comprising a full cycle for the tip displacement—the feedback loop is opened at a voltage of 300 mV and a current of 1 $\mu$A, and $\Delta z = 0$ is fixed to these feedback loop settings. The approach is performed over a molecule of **2** orientation (grey), but upon retraction this orientation has changed to **1** (black), as revealed by STM images (not shown). The rotation from **2** to **1** most probably occurred at displacements exceeding ≈−2.1 Å since both conductance curves coincide for displacements of <−2.1 Å (see the square in figure 13(b)). Upon tip retraction, conductance curves deviate from each other for displacements of >−2.1 Å. At zero displacement, the conductance of molecule **1** is slightly higher than the conductance of molecule **2** (see the inset of figure 13(b)). With $G_1 \approx 0.06\,G_0$, $G_2 \approx 0.04\,G_0$, and an apparent barrier height of $\Phi \approx 10$ eV (see above and [45]) we find a corresponding height difference of ≈0.15 Å which is close to the height difference inferred from cross-sectional profiles in constant-current STM images acquired at 300 mV, i.e., at the voltage at which the conductance traces in figure 13(b) were acquired. We notice that the displacement of ≈−0.23 Å at which the two conductance curves intersect (see the circle in the inset of figure 13) likewise reflects the difference in apparent height of the molecules.

Below we argue that the molecular rotation is mechanically induced whereas local heating plays a minor role in exciting rotations. An analysis of conductance curves for on $C_{60}$ at 300 mV [43] showed that energy dissipation in the tip–molecule junction leads to an effective heating which could cause rotation of the molecule. However, in the present experiments we varied the total power dissipated by a factor of 40. The probability for molecule rotation was found to be insensitive to the dissipated power. Although only a small fraction of the total power is dissipated directly at the molecule this finding suggests that thermal excitation alone is not the driving force for rotation. Moreover, the tunnelling current was not observed to be decisive for inducing rotation. We therefore suggest that mechanical contact with the tip causes $C_{60}$ to rotate.

Mechanically induced rotation explains that certain rotation angles are less frequently observed. For instance, switching a $C_{60}$ from **1** to **2** or vice versa requires a rotation by 20.6° while a smaller angle of 11.6° is required for a rotation from **1** to **5**. The apparent rotation by 90° in the surface plane can also be achieved by an out-of-plane rotation of 19.2° and 36.0° for the **1** and **2** orientations, respectively. The large angle needed for the apparent in-plane rotation of **2** molecules is consistent with the observed low frequency of this switching event. In the case of orientation **1** the apparent in-plane rotation results in a different adsorption geometry on the copper surface with now the carbon–carbon bond between the hexagon and the pentagon of the molecule parallel to the copper missing row. This specific orientation of molecules with orientation **1** is rarely observed, indicating a less favourable adsorption energy. This explains why this specific rotation is rare despite the relatively small angle needed to induce an apparent in-plane rotation of 90°. Switching between **3** and **4** orientations would require a relatively large rotation angle of 37.4°. In addition, their adsorption on top of the two missing copper rows leads to a stronger bonding of these molecules with the surface. The bonding is not limited to just the topmost copper atoms of the surface as for the three other configurations but also occurs with the copper atoms at the bottom of the missing row. The large angle needed for the rotation and the higher coordination of these configurations with the surface can then explain the absence of events of switching between **3** and **4** configurations upon elevated tip displacements.

## 5. Conclusion and outlook

State-of-the-art experiments addressing single-atom and single-molecule contact with the tip of a scanning tunnelling microscope were addressed. Owing to the imaging capability of the instrument the contacted objects as well as the tip can be characterized prior to and after contact. Therefore, precise and unambiguous information about the contact geometry is provided and the status of the contacting electrodes can be monitored. The objects to be contacted can moreover be chosen independently from the hosting substrate. The reviewed results showed that controlled and reproducible contact to surfaces, adsorbed atoms and molecules including spectroscopy in contact are feasible.

Future experiments will, for instance, provide spatially resolved contact conductance maps of complex molecules. The manipulation of structures at the nanometre scale and in contact with the tip will be addressed as well as the ballistic transport of spin-polarized electrons through magnetic structures [55]. Inelastically transferred electrons giving rise to phonon or photon [103, 104] excitation will be analysed by contact spectroscopy.

## Acknowledgments

Discussions and cooperation with A Garcia-Lekue, K Palotas, W Hofer (University of Liverpool), and Th Frederiksen, M Brandbyge (University of Denmark), and R Berndt (University of Kiel) are gratefully acknowledged. We thank C Cepek (Laboratorio Nazionale TASC, Italy) for providing clean $C_{60}$ molecules. Technical assistance from Ch Hamann (University of Kiel) for designing illustrative figures is acknowledged. Image processing was performed by Nanotec WSxM [105]. We thank the Deutsche Forschungsgemeinschaft for financial support.

## References

[1] Maxwell J C 1954 *A Treatise on Electricity and Magnetism* (New York: Dover)
[2] Sharvin Yu V 1965 A possible method for studying Fermi surfaces *Sov. Phys.—JETP* **21** 655

[3] Landauer R 1957 Spatial variation of currents and fields due to localized scatterers in metallic conduction *IBM J. Res. Dev.* **1** 223

[4] Büttiker M 1988 Coherent and sequential tunneling in series barriers *IBM J. Res. Dev.* **32** 63

[5] Brandbyge M and Jacobsen K W 1997 *Proc. NATO Advanced Research Workshop on Nanowires* (*NATO Advanced Studies Institute, Series E: Applied Sciences* vol 340) (Dordrecht: Kluwer)

[6] Bogachek E N, Zagoskin A N and Kulik I O 1990 Conductance jumps and magnetic flux quantization in ballistic point contacts *Sov. J. Low Temp. Phys.* **16** 796

[7] Torres J A, Pascual J L and Sáenz J J 1994 Theory of conduction through narrow constrictions in a three-dimensional electron gas *Phys. Rev.* B **49** 16581

[8] Brandbyge M, Schiøtz J, Sørensen M R, Stoltze P, Jacobsen K W, Nørskov J K, Olesen L, Lægsgaard E, Stensgaard I and Besenbacher F 1995 Quantized conductance in atom-sized wires between two metals *Phys. Rev.* B **52** 8499

[9] Brandbyge M, Jacobsen K W and Nørskov J K 1997 Scattering and conductance quantization in three-dimensional metal nanocontacts *Phys. Rev.* B **55** 2637

[10] Bürgi L 1999 Scanning tunneling microscopy as local probe of electron density, dynamics, and transport at metal surfaces *PhD Thesis* Ecole Polytechnique Fédérale de Lausanne

[11] Datta S 1995 *Electronic Transport in Mesoscopic Systems* (Cambridge: Cambridge University Press)

[12] Landauer R 1970 Electrical resistance of disordered one-dimensional lattices *Phil. Mag.* **21** 863

[13] Landauer R 1981 Can a length of perfect conductor have a resistance? *Phys. Lett.* A **85** 91

[14] Büttiker M, Imry Y, Landauer R and Pinhas S 1985 Generalized many-channel conductance formula with application to small rings *Phys. Rev.* B **31** 6207

[15] van Wees B J, van Houten H H, Beenakker C W J, Williamson J G, Kouwenhoven L P, van der Marel D and Foxon C T 1988 Quantized conductance of point contacts in a two-dimensional electron gas *Phys. Rev. Lett.* **60** 848

[16] Wharam D A, Thornton T J, Newbury R, Pepper M, Ahmed H, Frost J E F, Hosko D G, Peacock D C, Ritchie D A and Jones G A C 1988 One-dimensional transport and the quantisation of the ballistic resistance *J. Phys. C: Solid State Phys.* **21** L209

[17] Montie E A, Cosman E C, 't Hooft G W, van der Mark M B and Beenakker W J 1991 Observation of the optical analogue of quantized conductance of a point contact *Nature* **350** 594

[18] Gimzewski J K and Möller R 1987 Transition from the tunneling regime to point contact studied using scanning tunneling microscopy *Physica* B **36** 1284

[19] Jansen A G M, van Gelder A P and Wyder P 1980 Point-contact spectroscopy in metals *J. Phys. C: Solid State Phys.* **13** 6073

[20] García N and Escapa L 1989 Elastic oscillatory resistances of small contacts *Appl. Phys. Lett.* **54** 1418

[21] Pascual J I, Méndez J, Gómez-Herrero J, Baró A M, García N and Thien Binh V 1993 Quantum contact in gold nanostructures by scanning tunneling microscopy *Phys. Rev. Lett.* **71** 1852

[22] Moreland J and Ekin J W 1985 Electron tunneling experiments using Nb–Sn 'break' junctions *J. Appl. Phys.* **58** 3888

[23] Muller C J, van Ruitenbeek J M and de Jongh L J 1992 Experimental observation of the transition from weak link to tunnel junction *Physica* C **191** 485

[24] Muller C J, van Ruitenbeek J M and de Jongh L J 1992 Conductance and supercurrent discontinuities in atomic-scale metallic constrictions of variable width *Phys. Rev. Lett.* **69** 140

[25] Krans J M, van Ruitenbeek J M, Fisun V V, Yanson I K and de Jongh L J 1995 The signature of conductance quantization in metallic point contacts *Nature* **375** 767

[26] Olesen L, Lægsgaard E, Stensgaard I, Besenbacher F, Schiøtz J, Stoltze P, Jacobsen K W and Nørskov J K 1994 Quantized conductance in an atom-sized point contact *Phys. Rev. Lett.* **72** 2251

[27] Krans J M, Muller C J, van der Post N, Postma F R, Sutton A P, Todorov T N and van Ruitenbeek J M 1995 Comment on 'Quantized conductance in atom-sized point contact' *Phys. Rev. Lett.* **74** 2146

[28] Olesen L, Lægsgaard E, Stensgaard I, Besenbacher F, Schiøtz J, Stoltze P, Jacobsen K W and Nørskov J K 1995 Reply to Comment on 'Quantized conductance in atom-sized point contact' *Phys. Rev. Lett.* **74** 2147

[29] Landman U, Luedtke W D, Burnham N A and Colton R J 1990 Atomistic mechanisms and dynamics of adhesion, nanoindentation, and fracture *Science* **248** 454

[30] Todorov T N and Sutton A P 1993 Jumps in electronic conductance due to mechanical instabilities *Phys. Rev. Lett.* **70** 2138

[31] Agraït N, Rubio G and Vieira S 1995 Plastic deformation of nanometer-scale gold connective necks *Phys. Rev. Lett.* **74** 3995

[32] Rubio G, Agraït N and Vieira S 1996 Atomic-sized metallic contacts: mechanical properties and electronic transport *Phys. Rev. Lett.* **76** 2302

[33] Agraït N, Levy Yeyati A and van Ruitenbeek J M 2003 Quantum properties of atomic-sized conductors *Phys. Rep.* **377** 81

[34] Costa-Krämer J L, García N, García-Mochales P and Serena P A 1995 Nanowire formation in macroscopic metallic contacts: quantum mechanical conductance tapping a table top *Surf. Sci.* **342** L1144

[35] Landman U, Luedtke W D, Salisbury B E and Whetten R L 1996 Reversible manipulations of room temperature mechanical and quantum transport properties in nanowire junctions *Phys. Rev. Lett.* **77** 1362

[36] Hansen K, Lægsgaard E, Stensgaard I and Besenbacher F 1997 Quantized conductance in relays *Phys. Rev.* B **56** 2208

[37] Agraït N, Rodrigo J G and Vieira S 1993 Conductance steps and quantization in atomic-size contacts *Phys. Rev.* B **47** 12345

[38] Gai Z, He Y, Yu H and Yang W S 1996 Observation of conductance quantization of ballistic metallic point contacts at room temperature *Phys. Rev.* B **53** 1042

[39] Ohnishi H, Kondo Y and Takayanagi K 1998 Quantized conductance through individual rows of suspended gold atoms *Nature* **395** 780

[40] Erts D, Olin H, Ryen L, Olsson E and Thölén A 2000 Maxwell and Sharvin conductance in gold point contacts investigated using TEM–STM *Phys. Rev.* B **61** 12725

[41] Limot L, Kröger J, Berndt R, Garcia-Lekue A and Hofer W A 2005 Atom transfer and single-adatom contact *Phys. Rev. Lett.* **94** 126102

[42] Néel N, Kröger J, Limot L, Palotas K, Hofer W A and Berndt R 2007 Conductance and Kondo effect in a controlled single-atom contact *Phys. Rev. Lett.* **98** 016801

[43] Néel N, Kröger J, Limot L, Frederiksen T, Brandbyge M and Berndt R 2007 Controlled contact to a $C_{60}$ molecule *Phys. Rev. Lett.* **98** 065502

[44] Kröger J, Jensen H and Berndt R 2007 Conductance of tip–surface and tip–atom junction on Au(111) explored by a scanning tunnelling microscope *New J. Phys.* **9** 153

[45] Néel N, Kröger J, Limot L and Berndt R 2007 Conductance of single atoms and molecules studied with a scanning tunnelling microscope *Nanotechnology* **18** 044027

[46] Jensen H, Kröger J, Néel N and Berndt R 2007 Silver oligomer and single fullerene electronic properties revealed by a scanning tunnelling microscope *Eur. Phys. J.* D **45** 465

[47] Néel N, Limot L, Kröger J and Berndt R 2008 Rotation of $C_{60}$ in a single-molecule contact *Phys. Rev.* B **77** 125431

[48] Néel N, Kröger J, Limot L and Berndt R 2008 Probing the conductance of oriented molecules *Nano Lett.* at press

[49] Néel N, Kröger J, Limot L and Berndt R 2008 Conductance of single atoms and molecules studied with a scanning tunnelling microscope *J. Scann. Probe Microsc.* at press

[50] Kröger J 2008 Nonadiabatic effects on surfaces: Kohn anomaly, electronic damping of adsorbate vibrations, and local heating of single molecules *J. Phys.: Condens. Matter* at press

[51] Limot L, Maroutian T, Johansson P and Berndt R 2003 Surface-state Stark shift in a scanning tunneling microscope *Phys. Rev. Lett.* **91** 196801

[52] Kröger J, Limot L, Jensen H, Berndt R and Johansson P 2004 Stark effect in Au(111) and Cu(111) surface states *Phys. Rev.* B **70** 033401

[53] Simmons J G 1963 Generalized formula for the electric tunnel effect between similar electrodes separated by a thin insulating film *J. Appl. Phys.* **34** 1793

[54] Michelson H B 1977 The work function of the elements and its periodicity *J. Appl. Phys.* **48** 4729

[55] Néel N, Kröger J and Berndt R 2008 Local heating at a ferromagnet–metal interface, in preparation

[56] Hofer W A, Fisher A J, Wolkow R A and Grütter P 2001 Surface relaxations, current enhancements, and absolute distances in high resolution scanning tunneling microscopy *Phys. Rev. Lett.* **87** 236104

[57] Pethica J B and Sutton A P 1988 On the stability of a tip and flat at very small separation *J. Vac. Sci. Technol.* A **6** 2490

[58] Smith J R, Bozzolo G, Banerjea A and Ferrante J 1989 Avalanche in adhesion *Phys. Rev. Lett.* **63** 1269

[59] Scheer E, Agraït N, Cuevas J C, Levy Yeyati A, Ludoph B, Martín-Rodero A, Rubio Bollinger G, van Ruitenbeek J M and Urbina C 1998 The signature of chemical valence in the electrical conduction through a single-atom contact *Nature* **394** 154

[60] Cuevas J C, Levy Yeyati A, Martín-Rodero A, Rubio Bollinger G, Untiedt C and Agraít N 1998 Evolution of conducting channels in metallic atomic contacts under elastic deformation *Phys. Rev. Lett.* **81** 2990

[61] Yazdani A, Eigler D M and Lang N D 1996 Off-resonance conduction through atomic wires *Science* **272** 1921

[62] Hofer W A, Garcia-Lekue A and Brune H 2004 The role of surface elasticity in giant corrugations observed by scanning tunneling microscopes *Chem. Phys. Lett.* **397** 354

[63] Ludoph B, van der Post N, Bratus' E N, Bezuglyi E V, Shumeiko V S, Wendin G and van Ruitenbeek J M 2000 Multiple Andreev reflection in single atom niobium junctions *Phys. Rev.* B **61** 8561

[64] Li J, Schneider W-D, Berndt R and Delley B 1998 Kondo scattering observed at a single magnetic impurity *Phys. Rev. Lett.* **80** 2893

[65] Madhavan V, Chen W, Jamneala T, Crommie M F and Wingreen N S 1998 Tunneling into a single magnetic atom: spectroscopic evidence of the Kondo resonance *Science* **280** 567

[66] Újsághy O, Kroha J, Szunyogh L and Zawadowski A 2000 Theory of the Fano resonance in the STM tunneling density of states due to a single Kondo impurity *Phys. Rev. Lett.* **85** 2557

[67] Knorr N, Schneider M A, Diekhöner L, Wahl P and Kern K 2002 Kondo effect of single Co adatoms on Cu surfaces *Phys. Rev. Lett.* **88** 096804

[68] Fano U 1961 Effects of configuration interaction on intensities and phase shifts *Phys. Rev.* **124** 1866

[69] Anderson P W 1961 Localized magnetic states in metals *Phys. Rev.* **124** 41

[70] Hewson A C 1993 *The Kondo Problem to Heavy Fermions* (Cambridge: Cambridge University Press)

[71] Huang R Z, Stepanyuk V S, Klavsyuk A L, Hergert W, Bruno P and Kirschner J 2006 Atomic relaxations and magnetic states in a single-atom tunneling junction *Phys. Rev.* B **73** 153404

[72] Joachim C, Gimzewski J K, Schlittler R R and Chavy C 1995 Electronic transparence of a single $C_{60}$ molecule *Phys. Rev. Lett.* **74** 2102

[73] Abel M, Dmitriev A, Fasel R, Liu N, Barth J V and Kern K 2003 Scanning tunneling microscopy and x-ray photoelectron diffraction investigation of $C_{60}$ films on Cu(100) *Phys. Rev.* B **67** 245407

[74] Hou J G, Yang J, Wang H, Li Q, Zeng C, Lin H, Bing W, Chen D M and Zhu Q 1999 Identifying molecular orientation of individual $C_{60}$ on a Si(111)-(7 × 7) surface *Phys. Rev. Lett.* **83** 3001

[75] Lu X, Grobis M, Khoo K, Crommie M F and Louie S G 2003 Spatially mapping the spectral density of a single $C_{60}$ molecule *Phys. Rev. Lett.* **90** 096802

[76] Todorov T N 1998 Local heating in ballistic atomic-scale contacts *Phil. Mag.* B **77** 965

[77] Todorov T N, Hoekstra J and Sutton A P 2002 Current-induced embrittlement of atomic wires *Phys. Rev. Lett.* **86** 3606

[78] Chen Y C, Zwolak M and DiVentra M 2003 Local heating in nanoscale conductors *Nano Lett.* **3** 1691

[79] Tsutsui M, Kurokawa S and Sakai A 2007 Bias-induced local heating in atom-sized metal contacts at 77 K *Appl. Phys. Lett.* **90** 133121

[80] Huang Z, Xu B, Chen Y, DiVentra M and Tao N 2006 Measurement of current-induced local heating in a single molecule junction *Nano Lett.* **6** 1240

[81] Reed M A, Zhou C, Muller C J, Burgin T P and Tour J M 1997 Conductance of a molecular junction *Science* **278** 252

[82] Kergueris C, Bourgoin J-P, Palacin S, Esteve D, Urbina C, Magoga M and Joachim C 1999 Electron transport through a metal–molecule–metal junction *Phys. Rev.* B **59** 12505

[83] Reichert J, Ochs R, Beckmann D, Weber H B, Mayor M and von Löneysen H 2002 Driving current through single organic molecules *Phys. Rev. Lett.* **88** 176804

[84] Reichert J, Weber H B, Mayor M and von Löneysen H 2003 Low-temperature conductance measurements on single molecules *Appl. Phys. Lett.* **82** 4137

[85] Smit R H M, Noat Y, Untiedt C, Lang N D, van Hemert M C and van Ruitenbeek J M 2002 Measurement of the conductance of a hydrogen molecule *Nature* **419** 906

[86] Böhler T, Edtbauer A and Scheer E 2007 Conductance of individual $C_{60}$ molecules measured with controllable gold electrodes *Phys. Rev.* B **76** 125432

[87] Mujical V 1999 Electron transfer in molecules and molecular wires: geometry dependence, coherent transfer, and control *Adv. Chem. Phys.* **107** 403

[88] Moresco F, Meyer G, Rieder K-H, Tang H, Gourdon A and Joachim C 2001 Conformational changes of single molecules induced by scanning tunneling microscopy manipulation: a route to molecular switching *Phys. Rev. Lett.* **86** 672

[89] Dulić D, van der Molen S J, Koudernac T, Jonkman H T, de Jong J J D, Bowden T N, van Esch J, Feringa B L and van Wees B J 2003 One-way optoelectronic switching of photochromic molecules on gold *Phys. Rev. Lett.* **91** 207402

[90] Martin M, Lastapis M, Riedel D, Dujardin G, Mamatkulov M, Stauffer L and Sonnet Ph 2006 Mastering the molecular dynamics of a bistable molecule by single atom manipulation *Phys. Rev. Lett.* **97** 216103

[91] Venkataraman L, Klare J E, Nuckolls C, Hybertsen M S and Steigerwald M L 2006 Dependence of single-molecule junction conductance on molecular conformation *Nature* **442** 904

[92] Xue Y and Ratner M A 2003 Microscopic study of electrical transport through individual molecules with metallic contacts. I. Band lineup, voltage drop, and high-field transport *Phys. Rev.* B **68** 115406

[93] Xue Y and Ratner M A 2003 Microscopic study of electrical transport through individual molecules with metallic contacts. II. Effect of the interface structure *Phys. Rev.* B **68** 115407

[94] Untiedt C, Caturla M J, Calvo M R, Palacios J J, Segers R C and van Ruitenbeek J M 2007 Formation of a metallic contact: jump to contact revisited *Phys. Rev. Lett.* **98** 206801

[95] Eigler D M, Lutz C P and Rudge W E 1991 An atomic switch realized with the scanning tunnelling microscope *Nature* **352** 600

[96] Comstock M J, Cho J, Kirakosian A and Crommie M F 2005 Manipulation of azobenzene molecules on Au(111) using scanning tunneling microscopy *Phys. Rev.* B **72** 153414

[97] Qiu X H, Nazin G V and Ho W 2004 Mechanisms of reversible conformational transitions in a single molecule *Phys. Rev. Lett.* **93** 196806

[98] Henzl J, Mehlhorn M, Gawronski H, Rieder K-H and Morgenstern K 2006 Reversible *cis–trans*-isomerisierung eines einzelnen azobenzol-moleküls *Angew. Chem.* **118** 617

[99] Choi B-Y, Kahng S-J, Kim S, Kim H W, Song Y J, Ihm J and Kuk Y 2006 Conformational molecular switch of the azobenzene molecule: a scanning tunneling microscopy study *Phys. Rev. Lett.* **96** 156106

[100] Comstock M J, Levy N, Kirakosian A, Cho J, Lauterwasser F, Harvey J H, Strubbe D A, Fréchet J M, Trauner D, Louie S G and Crommie M F 2007 Reversible photomechanical switching of individual engineered molecules at a metallic surface *Phys. Rev. Lett.* **99** 038301

[101] Piva P G, DiLabio G A, Pitters J L, Zikovsky J, Rezeq M, Dogel S, Hofer W A and Wolkow R A 2006 Field regulation of single-molecule conductivity by a charged surface atom *Nature* **435** 658

[102] Keeling D L, Humphry M J, Fawcett R H J, Beton P H, Hobbs C and Kantorovich L 2005 Bond breaking coupled with translation in rolling of covalently bound molecules *Phys. Rev. Lett.* **94** 146104

[103] Berndt R, Gimzewski J K and Johansson P 1993 Electromagnetic interactions of metallic objects in nanometer proximity *Phys. Rev. Lett.* **71** 3493

[104] Aizpurua J, Hoffmann G, Apell S P and Berndt R 2002 Electromagnetic coupling on an atomic scale *Phys. Rev. Lett.* **89** 156830

[105] Gómez-Rodríguez J M, Colchero J, Gómez-Herrero J, Horcas I, Fernández R and Baro A M 2007 A software for scanning probe microscopy and a tool for nanotechnology *Rev. Sci. Instrum.* **78** 013705